CV.eDNA: A hybrid approach to invertebrate biomonitoring using computer vision and DNA metabarcoding

Keywords: Machine Learning; Deep Learning; Computer Vision; Image Classification; Convolutional Neural Networks; Ecological Monitoring; Species Identification; Macroecology

Jarrett D. Blair [1,2], Michael D. Weiser [3], Cameron Siler [3,4], Michael Kaspari [3,5], Sierra N. Smith [3,4,6], Jessica F. McLaughlin [3,4], Katie E. Marshall[1]

[1] Department of Zoology, University of British Columbia, Vancouver, BC V6T 1Z4, Canada
[2] Department of Ecoscience, Aarhus University, 8000 Aarhus C, Denmark
[3] School of Biological Sciences, University of Oklahoma, Norman, OK 73019-0235, USA
[4] Sam Noble Oklahoma Museum of Natural History, University of Oklahoma, Norman, OK 73072-7029, USA
[5] Conservation Ecology Center, Smithsonian's National Zoo and Conservation
[6] Department of Biology Institute, Front Royal, VA 22630, University of Texas at Arlington, Arlington, TX, 76019, USA.

Corresponding author: Jarrett Blair, Department of Ecoscience, Aarhus University, C.F. Møllers Allé 8, 8000 Aarhus C, Denmark, jarrett@ecos.au.dk

Abstract

1. Automated invertebrate classification using computer vision has shown significant potential to improve specimen processing efficiency. However, challenges such as invertebrate diversity and morphological similarity among taxa can make it difficult to infer fine-scale taxonomic classifications using computer vision. As a result, many invertebrate computer vision models are forced to make classifications at coarser levels, such as at family or order.
2. Here we propose a novel modular method to combine computer vision and bulk DNA metabarcoding specimen processing pipelines to improve the accuracy and taxonomic granularity of individual specimen classifications. To improve specimen classification accuracy, our methods use multimodal fusion models that combine image data with DNA-based assemblage data. To refine the taxonomic granularity of the model's classifications, our methods cross-references the classifications with DNA metabarcoding detections from bulk samples. We demonstrated these methods using a continental-scale, invertebrate bycatch dataset collected by the National Ecological Observatory Network. We also introduce the CV.eDNA R package, which aims to assist practitioners looking to implement our methods.
3. Using our methods, we reached a classification accuracy of 79.6% across the 17 taxa using real DNA assemblage data, and 83.6% when the assemblage data was "error-free", resulting in a 2.2% and 6.2% increase in accuracy when compared to a model trained using only images. After cross-referencing with the DNA metabarcoding detections, we improved taxonomic granularity in up to 72.2% of classifications, with up to 5.7% reaching species-level.

4. By providing computer vision models with coincident DNA assemblage data, and refining individual classifications using DNA metabarcoding detections, our methods the potential to greatly expand the capabilities of biological computer vision classifiers. Our methods allow computer vision classifiers to infer taxonomically fine-grained classifications when it would otherwise be difficult or impossible due to challenges of morphologic similarity or data scarcity. These methods are not limited to terrestrial invertebrates and could be applied in any instance where image and DNA metabarcoding data are concurrently collected.

1. Introduction

Computer vision has the potential to transform invertebrate ecology by automating estimations of invertebrate abundance, biomass, and diversity (Høye *et al.*, 2021; Schneider *et al.*, 2022; Blair *et al.*, 2024). However, accurately classifying invertebrate species using computer vision is challenging. This is partly due to the sheer diversity of invertebrates, as there are an estimated 7.5 million (~1.5 million named) terrestrial invertebrates species globally (Stork, 2018). This has led most invertebrate classification models to opt for coarser taxonomic granularity (e.g. order-level instead of species-level classifications) with relatively few unique classification groups (usually <50; (Ärje *et al.*, 2020; Blair *et al.*, 2022; Schneider *et al.*, 2022). However, ecology studies can involve hundreds or thousands of species, which poses a challenge for simpler machine vision techniques.

One way computer vision models have overcome the challenge of handling many thousands or millions of classification labels is by including additional data modalities such as contextual metadata (e.g. collection location) in computer vision models. The mobile app iNaturalist uses this spatiotemporal data in combination with user-submitted photos to classify nearly 80,000 taxa across the tree of life (Leary *et al.*, 2023). Other studies have also found substantial improvements to classification accuracy with multimodal models that include both metadata and images (Berg *et al.*, 2014; Terry, Roy and August, 2020; Blair *et al.*, 2022). However, despite the potential improvements in accuracy, there are several pitfalls to consider when including spatiotemporal metadata in a computer vision model. For one, spatiotemporal metadata is a lagging indicator of species habitat occupancy (i.e. the presence or absence of a species at a given place and time), and as such it is susceptible to data drift over time (Friedland, 2024). That is, spatiotemporal distributions of taxa change over time, but computer vision models can only

55 learn from past data. Unless a computer vision model is updated frequently with more recent
56 data, the species range distributions it has learned may quickly become outdated. Finally, when
57 dealing with many machine learning classes, spatiotemporal metadata does not solve the
58 challenge of gathering enough training data to sufficiently train a computer vision model (Beery
59 *et al.*, 2020). In short, studies that incorporate spatiotemporal metadata have shown that
60 supplemental, non-visual data can improve ecological computer vision models, but
61 spatiotemporal metadata itself has several potential drawbacks. In this study, we leverage an
62 alternative data stream that does not pose the same challenges associated with spatiotemporal
63 metadata: DNA metabarcoding.

64 DNA metabarcoding is an established tool in ecological research that allows for multiple species
65 to be identified from a single sample using high-throughput sequencing (Taberlet *et al.*, 2012;
66 Liu *et al.*, 2020). Using this method, DNA can be collected from the environment (eDNA) or
67 from preservative media (e.g. ethanol in insect bycatch samples), sequenced, and then used to
68 infer ecological metrics such as species richness and community composition (Marquina *et al.*,
69 2019; Weiser *et al.*, 2022). Due to its improved cost-effectiveness, DNA metabarcoding is
70 becoming more frequently used in large-scale studies where traditional morphological
71 identification techniques cannot keep up financially or logistically (Liu et al., 2020). However,
72 despite being an excellent tool for detecting occurrence at fine taxonomic granularity (even
73 below species-level; Stewart and Taylor, 2020), DNA metabarcoding cannot be used to reliably
74 estimate species abundance or biomass (Lamb *et al.*, 2019). Instead, eDNA metabarcoding is
75 more suitable for binary presence/absence detections of species. Additionally, while DNA
76 metabarcoding is generally reliable for taxonomic identifications, it is not exempt from false
77 positive and false negative detections (Guillera-Arroita *et al.*, 2017). Some examples of how this

may occur include DNA contamination and primer mis-priming (false-positives), or DNA degradation and insufficient sampling effort (false-negatives) (Guillera-Arroita *et al.*, 2017; Liu *et al.*, 2020). Therefore, while DNA metabarcoding offers considerable advantages for biodiversity assessment (e.g., species inventories, species richness) its limitations often necessitate the use of complementary indicators such as visual observations for other metrics (e.g., abundance, biomass) (Schneider et al., 2022).

Given DNA metabarcoding's ability to produce reliable fine-scale community composition data, and computer vision's ability to measure abundance and biomass at coarse taxonomic granularity, several studies have called for a synergistic classification pipeline that takes advantage of the strengths of each tool (Schneider *et al.*, 2022; Sys *et al.*, 2022; Badirli *et al.*, 2023). In theory, such a pipeline could leverage DNA metabarcoding's fine taxonomic granularity against computer vision's ability to infer specimen-level characteristics (identity, morphology, etc.) to make ecological inferences that would not be possible using either data stream on their own. DNA might also be a favourable alternative to spatiotemporal metadata, as it is a more direct and coincident indicator of species habitat occupancy, likely making it more resistant to data drift over time (Taberlet *et al.*, 2018). Despite the potential benefits of multimodal image-DNA classification models for ecological research, few studies have explored this approach. Additionally, proposed hybrid classification pipelines either leave the DNA and image data streams separate (Sys *et al.*, 2022), or sequence specimens individually, and thus do not take advantage of metabarcoding's ability to process bulk samples (Badirli *et al.*, 2023; Gong *et al.*, 2024).

Here we present a novel modular method for classifying invertebrate taxa that integrates DNA metabarcoding and computer vision. The objective of this hybrid approach is to improve the

accuracy and taxonomic granularity of computer vision classifications by adding concurrent community assemblage data derived from DNA metabarcoding into a bulk specimen classification pipeline (Figure 1). The combination of DNA and image data occurs twice throughout the pipeline: first during classification inference in the computer vision model, and then again as a post-processing step for the model's classifications. While developing this approach, we ask two primary questions: (1) How does error in DNA metabarcoding data affect the accuracy of the computer vision classification model? (2) What are the strengths and limitations of different classification granularity refinement methods? In addition to the case study we present here, we have also developed a GitHub repository to allow our methods to easily be adapted to other study systems (Blair, 2024). The repository introduces the CV.eDNA R package, which contains functions that assist with the implementation of our methods. The repository also includes demonstrative vignettes that walk through the data preparation, model training, and classification granularity refinement steps.

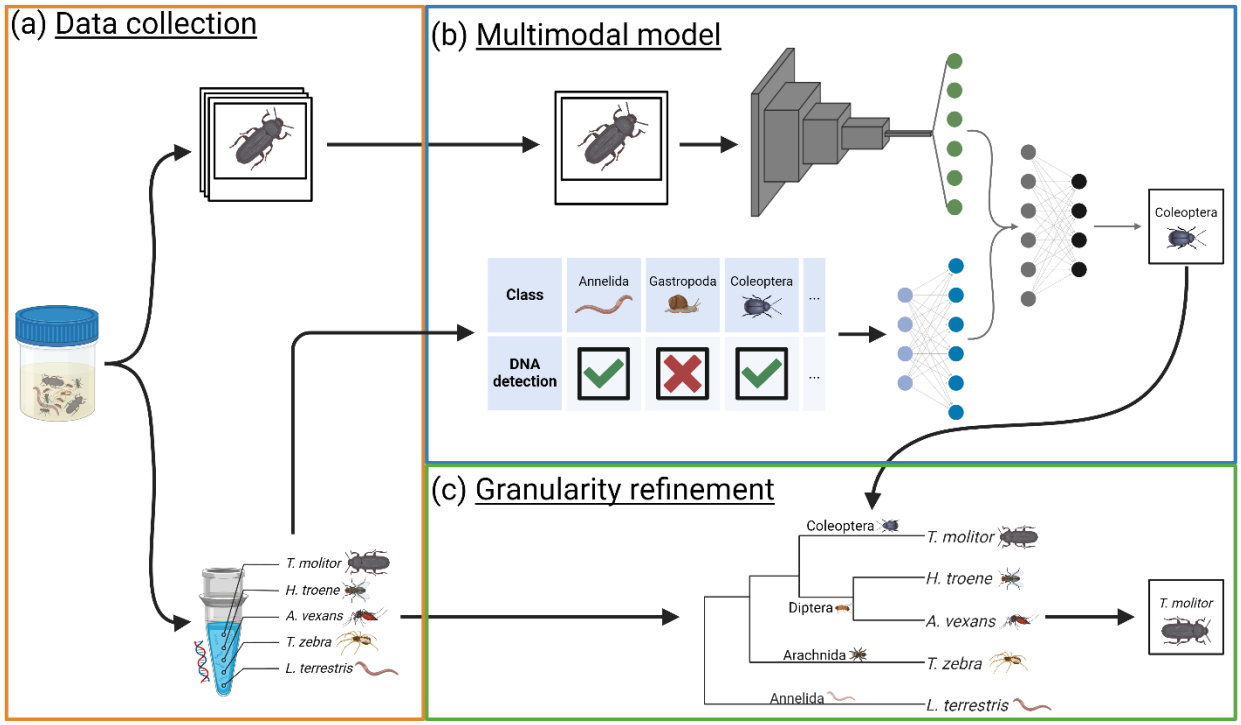

Figure 1: An overview of our methods for combining computer vision and DNA metabarcoding to improve the accuracy and taxonomic granularity of classifications. (a) Images and DNA metabarcoding data are collected concurrently from bulk samples. (b) Images and DNA assemblage data are used as input for a multimodal classification model. The features of the image input are extracted using a convolutional neural network. The DNA assemblage data provides presence/absence information for the model's known classes and is input as a binary vector into a dense neural network. The image features and the DNA features are concatenated and passed through one more dense layer before final classification in the softmax layer. The visual proportions of each layer have been simplified to ease interpretation and are not meant to be interpreted as 1:1 representations of the exact layer sizes. (c) By interpreting the DNA metabarcoding detections hierarchically and cross-referencing them with the model's classifications, the taxonomic granularity of the classifications can be refined.

2. Methods

2.1 Data collection

2.1.1 Specimen collection

Each year, the National Ecological Observatory Network (NEON) performs standardized pitfall trap array sampling across the United States, including Alaska, Hawaii, and Puerto Rico (Hoekman et al. 2017). The focal taxon of the pitfall trap array project are ground beetles

132 (Coleoptera: Carabidae), which are collected, identified, and counted by NEON staff members
133 once every two weeks during the growing season (defined as "the weeks when average minimum
134 temperatures exceed 4 °C for 10 days and ending when temperatures remain below 4 °C for the
135 same period", Kaspari et al., 2022). The remaining pitfall trap contents are set aside as
136 'Invertebrate Bycatch' and archived in 95% ethanol-filled 50 mL centrifuge tubes. Hereon, a
137 single collection period from a pitfall trap plot is referred to as a "sampling event".

138 The invertebrate bycatch specimens used in this research were taken from 56 NEON trap plots
139 from 27 sites (usually two plots per site; Figure S.1, S.2). Generally, we used three sampling
140 events per plot, selected at the beginning, middle, and end of each site's growing season. This
141 resulted in a total of 150 sampling events. All sampling events used here were collected in 2016
142 and processed in 2019. The focus of this project was to classify the invertebrate bycatch, so
143 ground beetles and non-invertebrate specimens were not considered.

144 2.1.2 Imaging

145 The contents of each 50mL centrifuge tube were spread out across a 20.32 cm ✕ 30.48 cm (8" ✕
146 12") white ceramic tile and photographed at a resolution of 729 pixels per mm^2, as described by
147 Weiser et al., 2021 (Figure S.3). Using the FIJI implementation of ImageJ (Schindelin et al.,
148 2012), each specimen was detected and cropped to its bounding box to produce a final image.

149 2.1.3 DNA extraction and metabarcoding

150 The DNA metabarcoding data used in this study was collected for Weiser et al., 2022, which
151 used the same sampling events described in Section 2.1.1. In brief, DNA metabarcoding was
152 conducted on a per-tube basis (Figure S.1). Ethanol from each falcon tube was filtered

individually (i.e., one filter per tube) and DNA was extracted from the filters using established protocols (Weiser et al., 2022). The cytochrome c oxidase I (COI) barcode region (141-254 base pairs) was then amplified using a two-step polymerase chain reaction (PCR) protocol and sequenced on an Illumina MiSeq. Three COI primers were used: 157, LCO, and Lep (Rennstam Rubbmark *et al.*, 2018, 2018; Hajibabaei *et al.*, 2019; Weiser *et al.*, 2022). Sequences were clustered into Operational Taxonomic Units (OTUs) and each OTU was assigned a taxonomic classification using NCBI BLASTn (Altschul *et al.*, 1990) and Integrated Taxonomic Information System (ITIS) (U.S. Geological Survey, 2013). Only sequences with ≥ 97% similarity between the OTU consensus sequence and the BLASTn search were used. See Weiser et al., 2022 for the full DNA extraction and metabarcoding methods.

In total, across all sampling events, there were 10,212 DNA metabarcoding detections. To align the DNA data with the imaging data, we removed any DNA detections from sampling events not included in the image dataset, as well as duplicate detections (i.e. multiple detections of the same taxon in a single sampling event, for example due to amplification using multiple primers). This yielded a final DNA metabarcoding dataset with 3,361 detections and 1,212 unique taxa, primarily consisting of family (369 detections; 85 unique), genus (468 detections; 183 unique), and species-level (2,471 detections; 922 unique) detections.

2.2 Data and labelling

2.2.1 Computer vision class labels

The taxonomic scope of the image and DNA metabarcoding data spanned three invertebrate phyla: Annelida, Arthropoda, and Mollusca. The specimen images were labelled by a single technician to the best of their ability (as described in Blair *et al.*, 2022). The final labels used for

our study ranged from order to phylum-level. Classes with a taxonomic granularity coarser than order-level but with no subtaxa present in the dataset (e.g. Phylum: Annelida) were included. Specimens labelled as nested classes at a taxonomic granularity coarser than order-level (Phylum: Arthropoda, Class: Insecta, and Class: Arachnida) were excluded, as these classes were primarily composed of "low quality" specimens (highly degraded, low image quality, partial specimens, etc.) that could not confidently be assigned finer level labels. Classes with fewer than 100 specimens in the dataset were also excluded. This resulted in a final image dataset with a total of 36,998 specimens across 17 machine learning classes (13 orders and one subclass, class, subphylum, and phylum; Figure S.4).

2.2.2 Hierarchical labels

Hierarchical labels created by the `refhier` and `longhier` functions in the CV.eDNA package contain taxonomic information at multiple levels (e.g. phylum to species) and can be assigned to images and sampling events (Table S.1, Table S.2). These labels are used as input for the classification granularity refinement methods (see Section 2.5).

In our case study, our image-based hierarchical labels contained taxonomic information at six levels from phylum to order-level for individual specimens (Table S.1). Our DNA-based hierarchical labels contained information at 13 levels from phylum to species for all DNA metabarcoding detections in each sampling event (Table S.2). The levels in the DNA-based hierarchical labels were phylum, subphylum, class, subclass, superorder, order, suborder, infraorder, superfamily, family, subfamily, genus, and species.

2.2.3 Binary assemblage data

196 The `get_assemblage` function in the CV.eDNA package generates binary assemblage data for
197 sampling events. This assemblage data can then be used as class priors or input features for
198 classification models (see Section 2.4). To generate this assemblage data, the function receives
199 DNA metabarcoding data or ground truth image metadata as input and outputs an *n*-element long
200 binary vector for each sampling event, where *n* is the number of classes known by the computer
201 vision model. If a given class is detected in a sampling event, its corresponding element is
202 assigned a score of 1, whereas it is assigned a score of 0 if it was not detected.

203 For our case study we generated two sets of binary assemblage data containing our 17 known
204 classes: one using detections from the image labels and one using detections from the DNA class
205 labels.

206 **2.3 Training and testing data split**

207 Quasi-replication occurs in machine learning datasets when the same or very similar data occur
208 in both the training and testing datasets. This violates the assumption of independence between
209 training and testing data and should be avoided to make valid inferences on the test data. The
210 DNA-based assemblage data presented a quasi-replication risk, as specimens from the same
211 sampling event would have the same assemblage data. To avoid quasi-replication, we split the
212 training and testing such that all specimens from a given sampling event were only included in
213 either the training or testing data. We set our target training:testing ratio to 85:15, and we
214 randomly added sampling events to the test dataset until the test dataset contained >15% of the
215 total number of specimens. The final train:test split was 31,381: 5,617 specimens and 122:28
216 sampling events.

217 **2.4 Classification models**

The objective of all the classification models was to accurately classify the class labels of individual specimen photos. Classification masks (Section 2.4.2) and multimodal fusion approaches (Section 2.4.3) were used to assess how classification accuracy changes when DNA-based assemblage data was added to the specimen classification pipeline. Both the classification masks and multimodal fusion models included "oracle" experiments, which used image-based assemblage data to simulate the performance of these methods under optimal conditions. We trained each classification model until the test dataset loss had not improved for 10 epochs (this does not include the classification masks, which did not go through the training process). Performance of each classification model was assessed using the original image labels as a ground truth. All code required for running these models can be found in the "Model_Scripts" subdirectory of our GitHub repository (Blair, 2024). All models were trained using an AMD Ryzen 7 5800X CPU, an NVIDIA GeForce RTX 4070 Ti GPU and 32 GB of RAM.

2.4.1 Baseline model

To evaluate model performance in the absence of DNA-based assemblage data, we trained a ResNet-50 (He et al., 2016) as a baseline model using only image data. The model was pre-trained using the ImageNet weights from He et al. (2016), and then fine-tuned using the NEON invertebrate bycatch image data. The ImageNet classification layer was removed and replaced with a new classification layer for our 17 classes. A batch normalization and dropout step were also implemented before the final classification layer. The model was trained using the Adam optimizer. The baseline model took 45 seconds per epoch to train, and 7 seconds to run inference on the test dataset.

2.4.2 Classification masks

240 If *a priori* probabilities for classes in a classification model are known, the outputs of the model
241 can be adjusted according to those probabilities to improve classification accuracy (Saerens,
242 Latinne and Decaestecker, 2002). We implement two variations of this technique which we call
243 "Naïve masks" (Section 2.4.2.1) and "Weighted Masks" (Section 2.4.2.2), whereby the class
244 priors are derived from a sample's DNA metabarcoding assemblage data. To apply classification
245 masks to our case study, each test dataset specimen's classification probabilities (i.e. softmax
246 layer values) from the baseline model were multiplied by their sampling event's classification
247 mask values. The class with the highest classification probability after applying the mask was
248 used as the final classification.

249 *2.4.2.1 Naïve mask*

250 When using a naïve mask, the softmax layer values for a given specimen are multiplied by the
251 specimen's sampling event's binary DNA metabarcoding assemblage data (generated using the
252 `get_assemblage` function). Thus, any classes not detected by the DNA metabarcoding in a
253 given sampling event have their respective softmax values set to 0, whereas the remaining
254 classes are unaffected. Naïve masks essentially operate as a "hard filter", where only classes
255 detected by the DNA metabarcoding can be classified by the model.

256 *2.4.2.2 Weighted mask*

257 "Hard" masks like the naïve mask, which set the softmax values of undetected classes to 0,
258 assume the DNA metabarcoding data is error-free. However, in reality, DNA metabarcoding can
259 have false positive and/or false negative detections (Taberlet *et al.*, 2018). A weighted mask is a
260 "softer" version of a naïve mask that allows classes not detected by the DNA metabarcoding to
261 still be classified. The weights for a weighted mask can be generated using the `get_weights`

262 function of the CV.eDNA package, and are calculated using the metabarcoding's true positive
263 rate (precision) and false negative rate (1 - recall) for each class. The DNA metabarcoding
264 precision and recall are calculated by comparing the DNA-based assemblage data to ground-truth
265 assemblage data (e.g. manually assigned image-based assemblage data). The weight that is
266 assigned to any given class in a sample is determined by whether or not the class was detected by
267 the DNA metabarcoding. Classes which have their DNA detected are assigned their
268 metabarcoding precision value, while classes which do not have their DNA detected are assigned
269 their 1 – recall value.

270 *2.4.2.3 Oracle mask*

271 As an oracle experiment to simulate a scenario where the DNA detections were in perfect
272 alignment with the image-based detections, we created a naive classification mask using the
273 image-based assemblage data. This mask was then applied to the classification output of the
274 baseline model. We did this to provide an upper-bound for the classification mask accuracy, and
275 to understand how DNA detection accuracy impacts specimen classification accuracy when
276 using classification masks.

277 <u>2.4.3 Multimodal fusion</u>

278 In deep learning, multimodal models can receive data from multiple modalities as input to
279 inform their classifications (Ramachandram and Taylor, 2017). For example, previous studies
280 have described multimodal classification models that receive images and raw DNA barcode
281 sequence data for individual specimens (Badirli *et al.*, 2023; Gong *et al.*, 2024). However, no
282 previous studies have described a multimodal model that combines specimen images with DNA
283 metabarcoding data from bulk samples. We achieve this by inputting DNA metabarcoding data

284 as tabular binary assemblage data, which is then combined with specimen image features using
285 intermediate fusion (Figure 1b). Intermediate fusion is an approach to building multimodal
286 models where data from each modality is input separately. The features from each input are then
287 extracted and concatenated prior to classification (Boulahia *et al.*, 2021). This allows the model
288 to contextualize a specimen's image features with class presence-absence data from the
289 specimen's sample. However, similar to the weighted mask approach (Section 2.4.2.2), the DNA
290 metabarcoding data does not act as a "hard filter", and the model can still make classifications
291 not detected by DNA metabarcoding. Additionally, because the assemblage data contains all
292 class detections for a given sample, the model can learn patterns of class co-occurrence to inform
293 its classifications.

294 In our case study, we paired our DNA metabarcoding assemblage data with individual specimens
295 based on their sampling event (the same approach as the classification masks described in
296 Section 2.4.2). After being input, features of the assemblage data were extracted using a single
297 fully-connected layer with batch normalization and dropout. Specimen images were fed through
298 the ResNet-50 architecture, which ultimately producing a flat feature layer. The image and
299 assemblage feature layers were then concatenated and passed through another fully-connected
300 layer with batch normalization and dropout before reaching the final classification layer. During
301 training, both sides of the multimodal model were trained simultaneously using the Adam
302 optimizer.

303 To understand the effect that DNA detection accuracy has on classification performance, we ran
304 three versions of the multimodal model using different types of assemblage data as input: (1)
305 using the DNA-based assemblage data, (2) using the image-based assemblage data, and (3) using
306 'zero-filled' assemblage data (all values in the assemblage data are set to zero). In all three

experiments the training and testing datasets used the same assemblage data type (i.e. DNA-based, image-based, or zero-filled). All three experiments used the same overall model architecture as described in Figure 1b. The purpose of the image-based assemblage experiment was to simulate the results of a model where the DNA detections perfectly aligned with the ground truth labels (i.e. an oracle experiment). The purpose of the zero-filled assemblage experiment was to control for differences in model architecture when comparing the multimodal models to models trained without DNA-based assemblage data, as the zero-filled data would provide no informative value to the model. The zero-filled assemblage data had the same dimensions as the other assemblage data (17 values for each sampling event). The multimodal models took 105 seconds per epoch to train, and 16 seconds to run inference on the test dataset.

2.5 Refining taxonomic granularity using DNA-based assemblage data

A strength of DNA metabarcoding is its ability to produce species-level detections. The `modelbias` and `dnabias` functions in our CV.eDNA package take advantage of this strength to refine the taxonomic granularity computer vision model classifications by cross-referencing them with the DNA metabarcoding detections (Figure 2). When using either function in cases where the model classifications and DNA metabarcoding detections agree on the presence of a class, the granularity of the classification improves until the number of subtaxa detected by the DNA metabarcoding was greater than 1 or the granularity reached species-level (Figure 2a,b). The functions differ in cases where the model classifications and DNA detections disagree on the presence of a class classified by the model. The model-biased method of the `modelbias` function is simple. In cases where the model and DNA metabarcoding disagree, the model classification remains unchanged (Figure 2c). When using the DNA-biased method of the `dnabias` function, the hierarchical label of the classified specimen is cross referenced with the

DNA metabarcoding hierarchical labels of the sampling event (Figure 2d, Table S.1, Table S.2). Starting from the original classification level, the granularity of the label is coarsened until an agreement between the model and DNA metabarcoding is reached. The taxonomic name at this level becomes an intermediate label, which is refined until the number of subtaxa detected by the DNA metabarcoding is greater than 1 or the granularity reached species-level.

To test the effectiveness of each method, we applied the model-biased and DNA-biased methods to the classifications of our DNA multimodal fusion model. A vignette for these methods can be found on our GitHub repository (Blair, 2024).

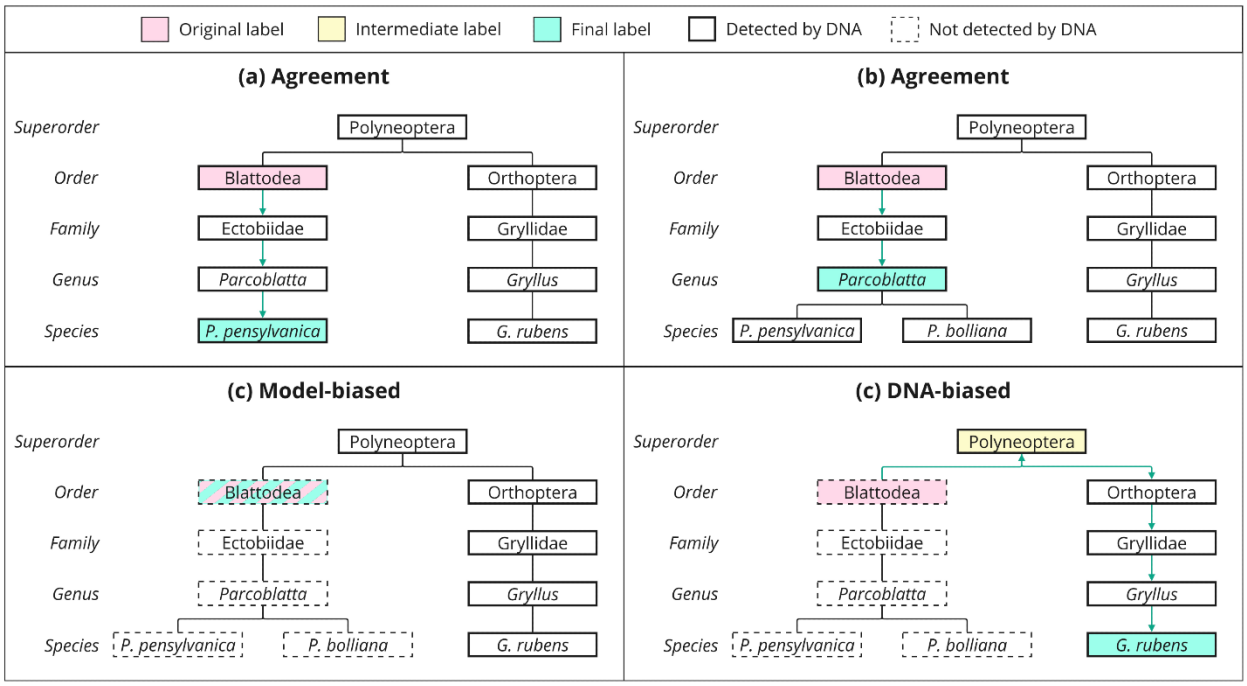

Figure 2: Four methods of changing a label's granularity using DNA detections. (a,b) When the classification label and DNA detections are in agreement about the presence of a class, granularity will be refined until the number of subtaxa detected by the DNA metabarcoding is > 1 or the classification reaches species level. (c) Under the model-biased approach, when the classification label and DNA metabarcoding do not agree on the presence of a class, the classification label remains unchanged. (d) Under the DNA-biased approach, when the classification label and DNA metabarcoding do not agree on the presence of a class, the granularity of the classification label is coarsened until a DNA detection for the class is found ("intermediate label"). The granularity of the intermediate label is then refined using the same rules as (a,b).

3. Results

3.1 DNA metabarcoding precision and recall

To generate the weights for the weighted mask, we calculated the DNA-based assemblage data's precision and recall for each class using the image-based assemblage data as the ground truth. This calculation only included sampling events from the training dataset. Across the 17 predicted classes, recall ranged from 0.905 to 0.000, with an average recall of 0.570. The weight for a negative detection was 1 - recall, so negative detection weights ranged from 1.000 to 0.095, with an average of 0.430. Two classes (Opilioacarida and Zygentoma) were never detected by the DNA. Across the 15 classes detected by the DNA, the average precision was 0.761. The precision and recall values per class are reported in Table S.3.

3.2 Classification accuracy

Compared to the baseline model, the DNA multimodal fusion model improved accuracy by 2.2% (79.6% vs 77.4%; Table 1). However, the DNA multimodal fusion model's accuracy was 1.0% lower than the zero-filled model's accuracy (80.6%). This suggests that some of the performance improvements seen in the multimodal fusion models could come from changes to the model architecture. The naïve classification mask recorded the lowest classification metrics, with an accuracy 22.6% below the baseline model (54.8%), and a top-3 accuracy of only 64.0%.

Our oracle experiments with image-based assemblage data performed better, with the multimodal fusion model reaching an average accuracy of 83.6% and a balanced accuracy (i.e. macro-averaged recall) of 0.713 (Table 2). The image-based naive mask accuracy was 25.8% better than the DNA-based naive mask, and 3.2% better than the baseline model. It also had the

highest top-3 accuracy across all experiments at 93.2%. Training dataset accuracy results for all non-mask experiments are reported in Table S.4.

Table 1: Performance metrics for experiments trained using DNA-based assemblage data, other than the baseline model, which was trained only using images, and the 'zero-filled' experiment, which replaced all assemblage data values with zero to control for the impact of model architecture. Underlined scores indicate they are the highest for a given metric.

Experiment	Accuracy	Balanced Accuracy	Top-3 Accuracy
Baseline	0.774	0.674	0.952
Naive mask	0.548	0.509	0.640
Weighted mask	0.764	0.666	0.950
Multimodal fusion	0.796	<u>0.680</u>	<u>0.957</u>
Multimodal fusion (zero-filled)	<u>0.806</u>	0.670	0.952

Table 2: Performance metrics for the oracle experiments using image-based assemblage data. These experiments used binary assemblage data taken from the ground truth specimen labels. Underlined scores indicate they are the highest for a given metric.

Experiment	Accuracy	Balanced Accuracy	Top-3 Accuracy
Mask	0.806	0.690	0.959
Multimodal fusion	<u>0.836</u>	<u>0.713</u>	<u>0.963</u>

3.3 Taxonomic granularity

Of the DNA multimodal fusion model classifications, 68.2% (3833/5617) were present in their corresponding sampling event's DNA assemblage data. Nonetheless, both approaches for handling disagreements between the DNA and classification model (model-biased or DNA-biased) improved the average taxonomic granularity of the classifications (Figure 3). Despite starting with no classifications finer than order-level, the DNA-biased approach resulted in 5.7% of classifications improving to species-level and the model-biased approach resulted in 5.1% of

the classifications improving to species-level. The DNA-biased approach was more effective overall at refining the granularity of classifications, with 72.2% of classifications becoming finer than their original classification, and 43.1% reaching at least family-level. In the model-biased approach, 51.7% of classifications improved their granularity, and 31.0% reached family-level or lower. When looking exclusively at classifications where the DNA assemblage data and multimodal fusion model classifications agreed on the presence of a class, 7.5% reached species level, 45.4% reached family-level or lower, and 75.7% became finer than their original classifications. Both the DNA-biased and model-biased approaches produced 89 unique final labels (Table S.5).

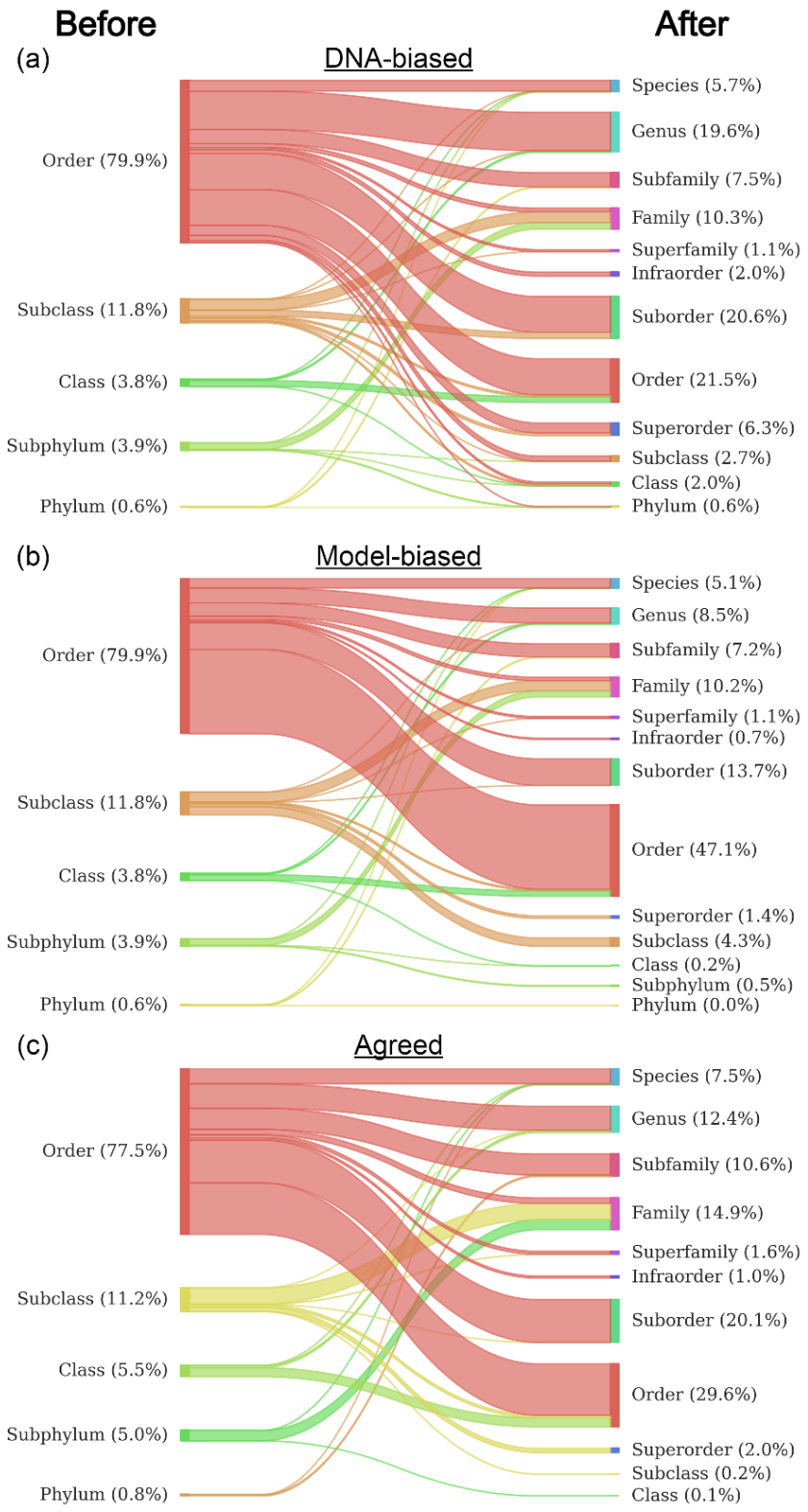

Figure 3: Sankey diagrams showing the change in taxonomic granularity before (left) and after (right) cross-referencing labels with the DNA detections. (a) DNA-biased approach. (b) Model-biased approach. (c) Results when the model classification and DNA detections agree on the presence of the labelled class.

4 Discussion

Here we show that combining concurrent DNA metabarcoding assemblage data with computer vision can improve the accuracy and taxonomic granularity of computer vision classifications. Unlike most classification pipeline enhancements which only focus on improving the ability to classify classes on which it was trained ("known classes"), this approach adds the ability for the pipeline to infer classifications beyond the model's usual taxonomic scope ("unknown classes"). Our methods could be applied to any study system where images and DNA metabarcoding data are collected concurrently, provided that the practitioners have labelled data to train their own classification model. To thoroughly explore the benefits and implications of our hybrid approach, we focused on the following two research questions.

4.1 How does DNA metabarcoding accuracy affect specimen classification accuracy?

The effect of metabarcoding accuracy on classification accuracy differed between the classification masks and the multimodal fusion models, illuminating a key difference between them: classification masks (as used in this study) do not take class co-occurrence into consideration, whereas the multimodal models do. Put another way, in a classification mask the only factor that directly influences the weight given to a class is the presence or absence of the class itself. Conversely, the neural networks of multimodal fusion models—with their fully-connected structure—allow the presence or absence of all classes to holistically influence each class's classification probability. This allows the model to use patterns of class co-occurrence to inform its classification decisions.

The different mechanisms used by classification masks and multimodal models are best demonstrated in Table 2, where the assemblage data was derived from the ground-truth image

labels. In the classification mask, the model's original classifications were exclusively based on image data, and any classifications that did not match their respective assemblage data were reclassified as the class with the highest softmax score that was present in the specimen's assemblage. Given that the assemblage data was derived from the ground truth labels, this mask acted as a sieve that filtered out any classes that could not possibly be the correct classification based on the assemblage data. As a result, it could only have a positive impact on accuracy. However, despite this, the multimodal fusion model still scored higher on all three metrics measured (top-1 accuracy, balanced accuracy, and top-3 accuracy). This implies that the multimodal fusion model was not just using the assemblage data as a filter, but that it provided additional contextual information (such as class co-occurrence or class exclusion) that further improved accuracy. Thus, due to the multimodal fusion model's ability to holistically evaluate occurrence data, and as illustrated through its superior performance compared to classification masks even under ideal conditions, multimodal fusion models are likely to be preferable in most use cases. This conclusion is reinforced by the results of Table 1, where both naïve and weighted masks showed negative effects on all classification performance metrics when the DNA-based assemblage data contained substantial amounts of error.

4.2 What are the strengths and limitations of each granularity refinement method?

Here we proposed two approaches for cross-referencing DNA metabarcoding data to achieve the novel ability of refining the taxonomic granularity of computer vision classifications. The two approaches differ in how they resolve disagreements between the detections of the DNA metabarcoding and computer vision classifications, with the model-biased approach favouring the computer vision classifications, and the DNA-biased approach favouring the DNA detections. As such, each approach has its own set of advantages and limitations.

443 Through the ability to coarsen granularity before refining it, the DNA-biased method can make
444 classifications outside of the taxonomy of the original classification model (Figure S.5).
445 Explained another way, the model-biased approach and traditional hierarchical classifiers (e.g.
446 Badirli *et al.*, 2023) can only adjust classifications "vertically" (i.e. to supertaxa or subtaxa of the
447 original classifications), but the DNA-biased approach can also adjust classifications "laterally"
448 to out-of-distribution taxa through a combination of classification coarsening and refining.
449 Classification of out-of-distribution taxa is usually only possible using feature embedding
450 learning methods such as zero-shot learning (Badirli *et al.*, 2021). An illustrative example of this
451 comes from the DNA-biased approach's detection of taxa within the insect order Psocodea (e.g.
452 *Valenzuela flavidus*; Table S.5). As Psocodea was not included as a class in our model, and our
453 model's finest taxonomic granularity was order-level, Psocodea's branch of the taxonomy was
454 only accessible through a "lateral" taxonomic adjustment (Figure S.5). As such, it was only
455 detected by the DNA-biased approach, and not the model-biased approach (Table S.5). In theory,
456 this extends the range of possible classifications to the full taxonomic scope of the genetic
457 reference database being used (e.g. GenBank, Barcode of Life, etc.) (Ratnasingham and Hebert,
458 2007; Sayers *et al.*, 2024). In practice, it is likely best to self-impose limits on how much the
459 DNA-biased method can coarsen granularity. In our case we limited ourselves to phylum, as we
460 were only interested in classifications within our three focal phyla.

461 While it does not have the same potential taxonomic scope of the DNA-biased approach, an
462 advantage of the model-biased approach is that the taxonomic granularity of the final
463 classification cannot be coarser than the original classification. Applied to the DNA multimodal
464 fusion model classifications, 9.9% of all classifications became coarser when the DNA-biased
465 method was used (Figure 3). While the DNA-biased method classified more specimens at

family-level or finer (43.1% vs 31.0%), the ability to coarsen granularity resulted in more classifications above order-level (11.7% vs 6.4%).

Even when granularity does not reach species, classifications that match with the DNA-based assemblage data still provide more information than what is typically output from a classification model. This is because we can also see the number and identity of subtaxa that the specimen could be according to the DNA metabarcoding detections. For example, if the DNA metabarcoding detected three species of the cricket genus *Gryllus* in a sample, we could say the label of a specimen that would otherwise be classified simply as "*Gryllus* indet." is actually one of three possible species of *Gryllus*, as detected by the DNA metabarcoding (e.g. *G. pennsylvanicus*, *G. rubens*, or *G. veletis*). This might also be useful for future developments to these methods, as the number of subtaxa detected by the DNA metabarcoding could be used to inform clustering algorithms that separate the specimens into morphotaxa.

Of course, the granularity of classifications matters little if they are not accurate. A caveat of our study is that we cannot verify the accuracy of granularity-refined classifications, as they are at lower taxonomic levels than our ground truth (human-classified) labels. However, we know that our classification models were more accurate than the DNA assemblage data when compared to our ground-truth labels. Thus, the DNA-biased method of refining granularity will likely add more error to the classifications than the model-biased approach. When deciding between the two methods, this is likely to be a determining factor: does the computer vision model or DNA metabarcoding contain more error?

4.3 Caveats and areas for future exploration

487 In an applied context, we cannot definitively conclude that image-DNA multimodal fusion
488 models as we present here improve specimen classification accuracy. This is primarily due to the
489 high rates of disagreement (or "error") between our DNA metabarcoding detections and image-
490 based detections. When comparing our three multimodal fusion experiments, the zero-filled
491 experiment had a top-1 accuracy 1.0% higher than the DNA-based assemblage data experiment,
492 but 3.0% less than the oracle experiment. This suggests that in an ideal situation where the DNA-
493 based assemblage data has low amounts of error (i.e. it is more similar to the image-based
494 assemblage data), image-DNA multimodal fusion models will positively impact classification
495 accuracy. However, when the DNA-based assemblage data contains substantial error, differences
496 in performance between the baseline and multimodal fusion models likely arise from changes in
497 the model's architecture.

498 Reconciling genetic-based and morphology-based data—the two chief methods for invertebrate
499 biodiversity monitoring—is a pressing need as previous studies have shown that assemblages
500 determined by visual classification usually differ from assemblages determined using DNA
501 metabarcoding. For example, Emmons *et al.* (2023) found that NEON benthic macroinvertebrate
502 samples classified by taxonomists only shared 59% of order-level detections with DNA
503 metabarcoding data derived from homogenized blends of the same samples. Similar results have
504 also been produced in other studies comparing metabarcoding methods to morphologic
505 identification (Remmel *et al.*, 2024; Salis *et al.*, 2024). Marquina *et al.*, (2019) also found that
506 different DNA sampling protocols can produce inconsistent assemblage data, as DNA
507 metabarcoded from ethanol vs homogenized blends of the same samples yielded significantly
508 different assemblage data, with both methods detecting taxa not detected by the other. Despite
509 these challenges, solutions to improve invertebrate detections using DNA metabarcoding are

being investigated. Proposed solutions range from changes in sampling methodology (e.g. strategically subsetting bulk samples; (Remmel *et al.*, 2024) to improvements in the completeness of publicly available DNA reference databases (Salis *et al.*, 2024). For the image-DNA multimodal fusion methods we propose here to be maximally effective, advances will need to be made in DNA metabarcoding methodology to limit false positive and false negative detections.

Beyond DNA metabarcoding accuracy, there are likely other factors that can impact the efficacy of our methods, such as the alpha and beta diversity of the sample assemblages. Lower alpha diversity and higher beta diversity should yield models with greater classification performance. Higher beta diversity would improve classification performance because the composition of the assemblages would be more heterogeneous, which is required for learnable patterns to emerge in the data. For example, our zero-filled assemblage experiment used data that was completely homogenous, as every sampling event had the same assemblage data, thus allowing no learnable patterns to emerge from the assemblage data. Conversely, lower alpha diversity would improve classification performance because more classes to be filtered out by the model. This is partially demonstrated by comparing the results of Blair *et al.* (2020) to the results we present here. In their study, which built classification models for NEON's carabid beetles, the authors applied classification masks to their models based on the detected ground beetle assemblages at each sampling site. On average, 2.93 out of 25 potential species (11.7%) were detected per site, resulting in an accuracy improvement of 10.9% (84.7% → 95.6%) after applying the classification masks. Comparatively, our image-based assemblages detected an average of 9.09 out of 17 potential classes (53.5%) per sampling event. When compared to the baseline model, this resulted in an accuracy improvement of 3.2% when using the classification mask and 6.2%

533 in the multimodal fusion model (Table 1, Table 2). Sample alpha diversity also has an impact on
534 the efficacy of the classification granularity refinement step. Higher alpha diversity increases the
535 odds that related taxa could present in the same sample, which can force our granularity
536 refinement methods to stop at a coarser taxonomic rank (Figure 2). Thus, sampling methods that
537 increase sample beta diversity (e.g. finer-grain class labels; Terlizzi *et al.*, 2009) and reduce
538 sample alpha diversity (e.g. smaller sample size; Chiu, 2023) will likely increase the efficacy of
539 image-DNA metabarcoding multimodal fusion classification pipelines.

540 **4.4 Broader applications and implications**

541 In this study, we used assemblage data derived from DNA metabarcoding to improve computer
542 vision classifications of terrestrial invertebrates. Previous studies (Badirli *et al.*, 2023; Gong *et*
543 *al.*, 2024) have paired images of specimens with their DNA barcode sequence as input for
544 multimodal classification models. However, this technique cannot be applied to DNA
545 metabarcoding data because samples are metabarcoded in bulk, so the metabarcoded sequences
546 cannot be paired with individual specimens. Our methods overcome this challenge by converting
547 DNA metabarcoding data to binary assemblage data, which can then be input to a multimodal
548 classification model. This advancement has several practical implications, as DNA
549 metabarcoding's ability to process bulk samples means that it is more time efficient, less
550 expensive, and produces less waste than individual specimen barcoding (Gueuning *et al.*, 2019).

551 Our method's ability to refine classification granularity, which is typically not possible in
552 computer vision, could improve the feasibility of building broad-scope, fine-grain classification
553 models (e.g. models spanning entire classes or phyla and capable of producing species-level
554 classifications). This typically requires vast amounts of training data, as training examples need

555 to be provided for every species. Using the approach that we present here, classifiers could be
556 trained at coarser taxonomic levels such as order or family and still have the potential to produce
557 species-level classifications. This would decrease the number of classes in the model, and thus
558 data needed to train it, by orders of magnitude. Hence, the synergy between DNA metabarcoding
559 and computer vision outlined in this study paves the way for new possibilities in computer vision
560 classification of taxa, with the potential for improved accuracy and granularity with far less data
561 dependency.

562 **Author contributions**

563 JDB and KEM conceived the ideas and designed methodology; JDB, MDW, CS, SNS, and JFM
564 collected data and helped refine ideas; JDB analysed the data and led the writing of the
565 manuscript. KEM and MK were principal investigators. All authors contributed critically to the
566 drafts and gave final approval for publication.

References

Altschul, S.F. *et al.* (1990) 'Basic local alignment search tool', *Journal of Molecular Biology*, 215(3), pp. 403–410. https://doi.org/10.1016/S0022-2836(05)80360-2.

Ärje, J. *et al.* (2020) 'Automatic image-based identification and biomass estimation of invertebrates', *Methods in Ecology and Evolution*, 11(8), pp. 922–931. https://doi.org/10.1111/2041-210X.13428.

Badirli, S. *et al.* (2021) 'Fine-Grained Zero-Shot Learning with DNA as Side Information', in *Advances in Neural Information Processing Systems*. Curran Associates, Inc., pp. 19352–19362. https://proceedings.neurips.cc/paper_files/paper/2021/hash/a18630ab1c3b9f14454cf70dc7114834-Abstract.html (Accessed: 24 July 2024).

Badirli, S. *et al.* (2023) 'Classifying the unknown: Insect identification with deep hierarchical Bayesian learning', *Methods in Ecology and Evolution*, 14(6), pp. 1515–1530. https://doi.org/10.1111/2041-210X.14104.

Beery, S. *et al.* (2020) 'Synthetic examples improve generalization for rare classes', in *Proceedings - 2020 IEEE Winter Conference on Applications of Computer Vision, WACV 2020*. https://doi.org/10.1109/WACV45572.2020.9093570.

Berg, T. *et al.* (2014) 'Birdsnap: Large-scale fine-grained visual categorization of birds', in *Proceedings of the IEEE Computer Society Conference on Computer Vision and Pattern Recognition*, pp. 2011–2018. https://doi.org/10.1109/CVPR.2014.259.

Blair, J. D. (2024) 'CV-eDNA-Hybrid'. https://github.com/Jarrett-Blair/CV-eDNA-Hybrid.

Blair, J.D. *et al.* (2020) 'Robust and simplified machine learning identification of pitfall trap-collected ground beetles at the continental scale', *Ecology and Evolution*, 10(23), pp. 13143–13153. https://doi.org/10.1002/ece3.6905.

Blair, J.D. *et al.* (2022) 'Embracing imperfection: Machine-assisted invertebrate classification in real-world datasets', *Ecological Informatics*, 72, p. 101896. https://doi.org/10.1016/j.ecoinf.2022.101896.

Blair, J.D. *et al.* (2024) 'A gentle introduction to computer vision-based specimen classification in ecological datasets', *Journal of Animal Ecology*, pp. 1365-2656.14042. https://doi.org/10.1111/1365-2656.14042.

Boulahia, S.Y. *et al.* (2021) 'Early, intermediate and late fusion strategies for robust deep learning-based multimodal action recognition', *Machine Vision and Applications*, 32(6), p. 121. https://doi.org/10.1007/s00138-021-01249-8.

Chiu, C. (2023) 'Sample coverage estimation, rarefaction, and extrapolation based on sample-based abundance data', *Ecology*, 104(8), p. e4099. https://doi.org/10.1002/ecy.4099.

601 Emmons, S.C. *et al.* (2023) 'DNA metabarcoding captures different macroinvertebrate
602 biodiversity than morphological identification approaches across a continental scale',
603 *Environmental DNA*, p. edn3.453. https://doi.org/10.1002/edn3.453.

604 Friedland, G. (2024) *Information-Driven Machine Learning: Data Science as an Engineering*
605 *Discipline*. 1st ed. Cham: Springer International Publishing AG.

606 Gong, Z. *et al.* (2024) 'CLIBD: Bridging Vision and Genomics for Biodiversity Monitoring at
607 Scale'. arXiv. https://doi.org/10.48550/ARXIV.2405.17537.

608 Gueuning, M. *et al.* (2019) 'Evaluating next-generation sequencing (NGS) methods for routine
609 monitoring of wild bees: Metabarcoding, mitogenomics or NGS barcoding', *Molecular Ecology*
610 *Resources*, 19(4), pp. 847–862. https://doi.org/10.1111/1755-0998.13013.

611 Guillera-Arroita, G. *et al.* (2017) 'Dealing with false-positive and false-negative errors about
612 species occurrence at multiple levels', *Methods in Ecology and Evolution*. Edited by R. McCrea,
613 8(9), pp. 1081–1091. https://doi.org/10.1111/2041-210X.12743.

614 Hajibabaei, M. *et al.* (2019) 'COI metabarcoding primer choice affects richness and recovery of
615 indicator taxa in freshwater systems', *PLOS ONE*. Edited by A. Ramaiah, 14(9), p. e0220953.
616 https://doi.org/10.1371/journal.pone.0220953.

617 He, K. *et al.* (2016) 'Deep residual learning for image recognition', in *Proceedings of the IEEE*
618 *Computer Society Conference on Computer Vision and Pattern Recognition*.
619 https://doi.org/10.1109/CVPR.2016.90.

620 Høye, T.T. *et al.* (2021) 'Deep learning and computer vision will transform entomology',
621 *Proceedings of the National Academy of Sciences of the United States of America*, 118(2).
622 https://doi.org/10.1073/PNAS.2002545117.

623 Kaspari, M. *et al.* (2022) 'Activity density at a continental scale: What drives invertebrate
624 biomass moving across the soil surface?', *Ecology*, 103(1), p. e03542.
625 https://doi.org/10.1002/ecy.3542.

626 Lamb, P.D. *et al.* (2019) 'How quantitative is metabarcoding: A meta-analytical approach',
627 *Molecular Ecology*, 28(2), pp. 420–430. https://doi.org/10.1111/mec.14920.

628 Leary, P. *et al.* (2023) 'inatVisionAPI'. https://github.com/inaturalist/inatVisionAPI (Accessed:
629 26 September 2023).

630 Liu, M. *et al.* (2020) 'A practical guide to DNA metabarcoding for entomological ecologists',
631 *Ecological Entomology*, 45(3), pp. 373–385. https://doi.org/10.1111/een.12831.

632 Marquina, D. *et al.* (2019) 'Establishing arthropod community composition using
633 metabarcoding: Surprising inconsistencies between soil samples and preservative ethanol and
634 homogenate from Malaise trap catches', *Molecular Ecology Resources*, 19(6), pp. 1516–1530.
635 https://doi.org/10.1111/1755-0998.13071.

636 Ramachandram, D. and Taylor, G.W. (2017) 'Deep Multimodal Learning: A Survey on Recent
637 Advances and Trends', *IEEE Signal Processing Magazine*, 34(6), pp. 96–108.
638 https://doi.org/10.1109/MSP.2017.2738401.

639 Ratnasingham, S. and Hebert, P.D.N. (2007) 'BOLD : The Barcode of Life Data System
640 (http://www.barcodinglife.org)', *Molecular Ecology Notes*, 7(3), pp. 355–364.
641 https://doi.org/10.1111/j.1471-8286.2007.01678.x.

642 Remmel, N. *et al.* (2024) 'DNA metabarcoding and morphological identification reveal similar
643 richness, taxonomic composition and body size patterns among flying insect communities',
644 *Insect Conservation and Diversity*, 17(3), pp. 449–463. https://doi.org/10.1111/icad.12710.

645 Rennstam Rubbmark, O. *et al.* (2018) 'A broadly applicable COI primer pair and an efficient
646 single-tube amplicon library preparation protocol for metabarcoding', *Ecology and Evolution*,
647 8(24), pp. 12335–12350. https://doi.org/10.1002/ece3.4520.

648 Saerens, M., Latinne, P. and Decaestecker, C. (2002) 'Adjusting the Outputs of a Classifier to
649 New a *Priori* Probabilities: A Simple Procedure', *Neural Computation*, 14(1), pp. 21–41.
650 https://doi.org/10.1162/089976602753284446.

651 Salis, R. *et al.* (2024) 'Performance of DNA metabarcoding, standard barcoding and
652 morphological approaches in the identification of insect biodiversity', *Molecular Ecology*
653 *Resources*, 24(8), p. e14018. https://doi.org/10.1111/1755-0998.14018.

654 Sayers, E.W. *et al.* (2024) 'GenBank 2024 Update', *Nucleic Acids Research*, 52(D1), pp. D134–
655 D137. https://doi.org/10.1093/nar/gkad903.

656 Schneider, S. *et al.* (2022) 'Bulk arthropod abundance, biomass and diversity estimation using
657 deep learning for computer vision', *Methods in Ecology and Evolution*, 13(2), pp. 346–357.
658 https://doi.org/10.1111/2041-210X.13769.

659 Stewart, K.A. and Taylor, S.A. (2020) 'Leveraging eDNA to expand the study of hybrid zones',
660 *Molecular Ecology*, 29(15), pp. 2768–2776. https://doi.org/10.1111/mec.15514.

661 Stork, N.E. (2018) 'How Many Species of Insects and Other Terrestrial Arthropods Are There on
662 Earth?', *Annual Review of Entomology*, 63(1), pp. 31–45. https://doi.org/10.1146/annurev-ento-
663 020117-043348.

664 Sys, S. *et al.* (2022) 'COLLEMBOLAI , a macrophotography and computer vision workflow to
665 digitize and characterize samples of soil invertebrate communities preserved in fluid', *Methods*
666 *in Ecology and Evolution*, 13(12), pp. 2729–2742. https://doi.org/10.1111/2041-210X.14001.

667 Taberlet, P. *et al.* (2012) 'Towards next-generation biodiversity assessment using DNA
668 metabarcoding', *Molecular Ecology*, 21(8), pp. 2045–2050. https://doi.org/10.1111/j.1365-
669 294X.2012.05470.x.

670 Taberlet, P. *et al.* (2018) *Environmental DNA: for biodiversity research and monitoring*. First
671 edition. Oxford, United Kingdom: Oxford University Press.

Terlizzi, A. *et al.* (2009) 'Beta diversity and taxonomic sufficiency: Do higher-level taxa reflect heterogeneity in species composition?', *Diversity and Distributions*, 15(3), pp. 450–458. https://doi.org/10.1111/j.1472-4642.2008.00551.x.

Terry, J.C.D., Roy, H.E. and August, T.A. (2020) 'Thinking like a naturalist: Enhancing computer vision of citizen science images by harnessing contextual data', *Methods in Ecology and Evolution*, 11(2), pp. 303–315. https://doi.org/10.1111/2041-210X.13335.

U.S. Geological Survey (2013) 'Integrated Taxonomic Information System (ITIS)'. https://doi.org/10.5066/F7KH0KBK.

Weiser, M.D. *et al.* (2021) *Batch extraction of morphological and color metrics from invertebrate samples*, *protocols.io*. https://doi.org/dx.doi.org/10.17504/protocols.io.byt4pwqw.

Weiser, M.D. *et al.* (2022) 'Robust metagenomic evidence that local assemblage richness increases with latitude in ground-active invertebrates of North America', *Oikos*, 2022(8), p. e08791. https://doi.org/10.1111/oik.08791.